RESEARCH ARTICLE

CNS high-grade neuroepithelial tumor with *BCOR* internal tandem duplication: a comparison with its counterparts in the kidney and soft tissue

Yuka Yoshida[1]; Sumihito Nobusawa [1]; Satoshi Nakata[1]; Mitsutoshi Nakada[2]; Yoshiki Arakawa[3]; Yohei Mineharu[3]; Yasuo Sugita[4]; Takako Yoshioka[5]; Asuka Araki[6]; Yuichiro Sato[7]; Hideo Takeshima[8]; Masahiko Okada[9]; Akira Nishi[10]; Tatsuya Yamazaki[1]; Kenichi Kohashi[11]; Yoshinao Oda[11]; Junko Hirato[12,13]; Hideaki Yokoo[1]

[1] Department of Human Pathology, Gunma University Graduate School of Medicine, Maebashi, Japan.

[2] Department of Neurosurgery, Graduate School of Medical Science, Kanazawa University, Kanazawa, Japan.

[3] Department of Neurosurgery, Kyoto University Graduate School of Medicine, Kyoto, Japan.

[4] Department of Pathology, Kurume University School of Medicine, Kurume, Japan.

[5] Department of Pathology, National Center for Child Health and Development, Tokyo, Japan.

[6] Department of Organ Pathology, Shimane University School of Medicine, Izumo, Japan.

[7] Department of Diagnostic Pathology; [8] Department of Neurosurgery, Division of Clinical Neuroscience, Faculty of Medicine, University of Miyazaki, Miyazaki, Japan.

[9] Department of Pediatrics, Nagasaki University School of Medicine, Nagasaki, Japan.

[10] Department of Pediatric Surgery, Gunma Children's Medical Center, Shibukawa, Japan.

[11] Department of Anatomic Pathology, Graduate School of Medical Sciences, Kyushu University, Fukuoka, Japan.

[12] Department of Pathology, Gunma University Hospital, Maebashi, Japan.

[13] Department of Clinical Laboratory, Gunma Children's Medical Center, Shibukawa, Japan.

Abstract

Central nervous system high-grade neuroepithelial tumors with *BCOR* alteration (CNS HGNET-BCOR) are a recently reported rare entity, identified as a small fraction of tumors previously institutionally diagnosed as so-called CNS primitive neuroectodermal tumors. Their genetic characteristic is a somatic internal tandem duplication in the 3′ end of *BCOR* (*BCOR* ITD), which has also been found in clear cell sarcomas of the kidney (CCSK) and soft tissue undifferentiated round cell sarcomas/primitive myxoid mesenchymal tumors of infancy (URCS/PMMTI), and these *BCOR* ITD-positive tumors have been reported to share similar pathological features. In this study, we performed a clinicopathological and molecular analysis of six cases of CNS HGNET-BCOR, and compared them with their counterparts in the kidney and soft tissue. Although these tumors had histologically similar structural patterns and characteristic monotonous nuclei with fine chromatin, CNS HGNET-BCOR exhibited glial cell morphology, ependymoma-like perivascular pseudorosettes and palisading necrosis, whereas these features were not evident in CCSK or URCS/PMMTI. Immunohistochemically, diffuse staining of Olig2 with a mixture of varying degrees of intensity, and only focal staining of GFAP, S-100 protein and synaptophysin were observed in CNS HGNET-BCOR, whereas these common neuroepithelial markers were negative in CCSK and URCS/PMMTI. Therefore, although CNS HGNET-BCOR, CCSK and URCS/PMMTI may constitute a group of *BCOR* ITD-positive tumors, only CNS HGNET-BCOR has histological features suggestive of glial differentiation. In conclusion, we think CNS HGNET-BCOR are a certain type of neuroepithelial tumor relatively close to glioma, not CCSK or URCS/PMMTI occurring in the CNS.

INTRODUCTION

Recently, Sturm *et al* reported that, based on the comprehensive (epi)genome-wide analyses, tumors previously institutionally diagnosed as so-called central nervous system primitive neuroectodermal tumors (CNS-PNET) were mostly reclassified as other well-defined tumor entities, such as high-grade gliomas with *IDH1/2* or *H3F3A* mutation, medulloblastomas (WNT, SHH, group 3 or group 4) or ependymomas with *RELA* or *YAP* fusion, and furthermore, found four new, unrecognized tumor types in the remaining groups: CNS neuroblastoma with *FOXR2* activation, CNS Ewing sarcoma

family tumor with *CIC* alteration, CNS high-grade neuroepithelial tumor (HGNET) with *MN1* alteration and CNS HGNET with *BCOR* alteration (CNS HGNET-BCOR) (25). In the CNS HGNET-BCOR entity, somatic internal tandem duplications (ITD) in the 3′ end (exon 15) of the *BCOR* gene were recurrently identified in 14 tumors, and *BCOR* mRNA overexpression was noted (25). Clinically, CNS HGNET-BCOR predominantly affected children and occurred mostly in the supratentorial but occasionally in the infratentorial region, and preliminary survival data suggested poor overall survival (25). These tumors were reported to present as well-circumscribed masses, to frequently histologically exhibit fibrillary cytoplasmic processes suggesting glial differentiation, and to often have ependymoma-like perivascular pseudorosettes (25). Immunohistochemically, the tumor cells frequently exhibited GFAP expression, but neuronal antigen expression was focal or absent (25).

BCOR ITD was first described in clear cell sarcoma of the kidney (CCSK) by Ueno-Yokohata *et al* (26). CCSK are aggressive childhood tumors that account for 2%–5% of primary renal neoplasms in children (8, 10). Histologically, CCSK display various morphological patterns; the classic appearance is composed of monotonous round to oval cells with characteristic nuclei containing fine chromatin and indistinct nucleoli, and delicate branching vessels with a chicken-wire appearance separating the tumor cells into nests or cords, with the less common morphologies being a myxoid background, sclerosing stroma, acinar or rosette-like formation or spindle cell cytomorphology (2). *BCOR* ITD has been identified as a recurrent abnormality in approximately 85% of CCSK (3, 14, 23, 26), and *YWHAE-NUTM2* fusion has been mutually exclusively found in 9%–12% of the cases (14, 19). Both CCSK with *BCOR* ITD and those with *YWHAE-NUTM2* fusion were reported to exhibit nuclear expression of BCOR (13), suggesting that these different genetic abnormalities may trigger a similar downstream pathway (12).

Soft tissue undifferentiated round cell sarcomas (URCS) are a heterogenous group of tumors that are histologically composed of tumor cells with monomorphous round nuclei and scant cytoplasm, demonstrating varying genetic abnormalities and clinical features. Recently, *BCOR* ITD was identified in a subset of URCS in infants and in nearly all so-called primitive myxoid mesenchymal tumors of infancy (PMMTI) (12, 24). Moreover, URCS/PMMTI with *BCOR* ITD and URCS with other *BCOR*-related fusions or *YWHAE-NUTM2* fusion have been found to share similar histological features and nuclear expression of BCOR with CCSK (12, 13). Recently, Chiang *et al* reported that a high-grade endometrial stromal sarcoma in a 25-year-old female harbored *BCOR* ITD, and the tumor was histologically similar with high-grade endometrial stromal sarcomas with *YWHAE-NUTM2* fusion (6).

Since Sturm *et al* first introduced CNS HGNET-BCOR, only five cases have been reported (1, 16, 20). Appay R *et al* examined three cases of cerebellar HGNET-BCOR, and noted the possibility that these tumors represent a local variant of the same entity as CCSK and URCS/PMMTI with *BCOR* ITD because they all shared pathological features, *BCOR* ITD and BCOR nuclear immunoreactivity (1). In the current report, we performed a clinicopathological and molecular analysis of six new cases of CNS HGNET-BCOR and compared them with their counterparts in the kidney and soft tissue to better characterize this emerging entity.

MATERIALS AND METHODS

Tumor samples

Six cases of HGNET-BCOR were collected for this study (Table 1). Four and two cases were from the consultation files of the authors, JH and SN, respectively. We searched the consultation archives for "unclassified high-grade neuroepithelial tumors" composed of tumor cells with monotonous round to oval nuclei containing fine chromatin, a characteristic feature of CCSK and URCS/PMMTI with *BCOR* ITD reported (12), showing a solid growth pattern. We found six such cases and analyzed them for *BCOR* ITD, and the ITD was detected in all six cases (for details see "RESULTS"). For reference, five CCSK cases and one URCS/PMMTI case were collected from the pathology archives of the Department of Anatomic Pathology, Kyushu University, and Department of Clinical Laboratory, Gunma Children's Medical Center, respectively. Sections for histological and genetic analyses were prepared from formalin-fixed paraffin-embedded (FFPE) tissue specimens. This study was conducted in accordance with the Gunma University Ethical Committee.

Conventional histological analysis

Three-micrometer-thick tissue sections were cut and stained with hematoxylin and eosin. Immunohistochemical staining was performed on FFPE tissue sections. Primary antibodies directed against the following antigens were applied: BCOR (C-10; 1:100; Santa Cruz Biotechnology, Dallas, TX, USA), vimentin (V9; 1:200; Dako, Glostrup, Denmark), glial fibrillary acidic protein (GFAP) (1:5000) (18), Olig2 (1:5000) (27), S-100 protein (1:10000) (18), synaptophysin (27G12; 1:200; Leica Microsystems, Newcastle, UK), neurofilament protein (RMdO-20; 1:100; Thermo Fisher Scientific, MA, USA), epithelial membrane antigen (EMA) (E29; 1:100; Dako), BAF47/INI1 (BAF47; 1:100; BD Bioscience, San Jose, CA, USA), BRG1 (polyclonal; 1:1000; Millipore, Temecula, CA, USA) and Ki-67 (MIB-1; 1:100; Dako). For coloration, a commercially available biotin-streptavidin immunoperoxidase kit (Histofine, Nichirei, Tokyo, Japan) and diaminobenzidine were used. For BCOR staining, spermatogonia in the seminiferous tubules of the normal testis were used as positive controls (13).

For BCOR, vimentin, GFAP, Olig2, S-100 protein, synaptophysin and neurofilament protein, the intensity of the staining was graded as negative, weak, moderate or strong, and the extent was scored as follows: −, completely negative; 1+, <10% of tumor cells are positive; 2+, 10%–50% of tumor cells are positive; 3+, >50% of tumor cells are positive.

PCR and direct DNA sequencing of *BCOR* exon 15

Genomic DNA was extracted from FFPE tissue sections as previously described (11), and was amplified and sequenced using previously described primer sets for detecting *BCOR* ITD (12). PCR products were analyzed by agarose gel electrophoresis, and were then sequenced on a 3130xl Genetic Analyzer (Applied Biosystems, Foster City, CA, USA) with the Big Dye Terminator v.1.1 Cycle Sequencing Kit (Applied Biosystems) following standard procedures.

Table 1. Case list of CNS HGNET-BCOR with clinical features.

Case	Age/Sex	Location	Surgery	Radiation, dose	Chemotherapy	Local recurrence	Dissemination	Extra CNS metastasis	Clinical outcomes
1	11 mo/M	Cerebellar hemisphere	Partial resection	No	No	No (regrowth)	No	No	Dead, 2 months
2	6 y.o./M	Cerebellar hemisphere	Total resection	focal, 55.8 Gy/31 fr	No	Yes	No	Subcutaneous seeding	–
(Rec1)		Posterior fossa +subcutaneous	Total resection	IMRT, 59.4 Gy/33 fr	CDDP+VP16+CPA	Yes	No	No	–
(Rec2)		Posterior fossa	Resection	electron irradiation, 54 Gy	No	Yes	Yes	No	–
(Rec3)		Cerebellar hemisphere	No	SRT, 40 Gy/10 fr	Bevacizmab		Yes		Dead, 36 months
3	6 y.o./M	Left temporal lobe	Total resection	CSI, 24 Gy/16 fr +focal, 27.2/17 fr	multiagents*, PBSCT, VP16	No	No	No	Alive at 26 months
4	3 y.o./F	Cerebellar hemisphere	Total resection	NA	NA	NA	NA	NA	NA
5	7 mo/M	Cerebellar hemisphere	Total resection	No	No	Yes	No	No	–
(Rec1)		Cerebellar hemisphere	Total resection	No	IT-MTX	Yes	No	No	–
(Rec2)		Cerebellar hemisphere	Total resection	focal+posterior fossa, 50.4 Gy/28 fr	IT-MTX, IT-topotecan, high-dose chemotherapy, PBSCT	No	No	No	Alive at 37 months
6	22 y.o./M	Cerebellopontine angle	Partial resection	No	CDDP+VP16	No (regrowth)	No	No	Dead, 2 months

*Multiagents including CDDP, CPA, VP16.

Abbreviations: CNS HGNET-BCOR = central nervous system high-grade neuroepithelial tumor with *BCOR* alteration; y.o. = years old; mo = months; M = male; F = female; NA = not available; ND = not determined; IMRT = intensity modulated radiation therapy; SRT = stereotactic radiotherapy; CSI = craniospinal irradiation; VCR = vincristine; CDDP = cisplatin; VP16 = etoposide; CPA = cyclophosphamide; IT-MTX = intrathecal methotrexate; IT-topotecan = intrathecal topotecan; PBSCT = peripheral blood stem cell transplantation.
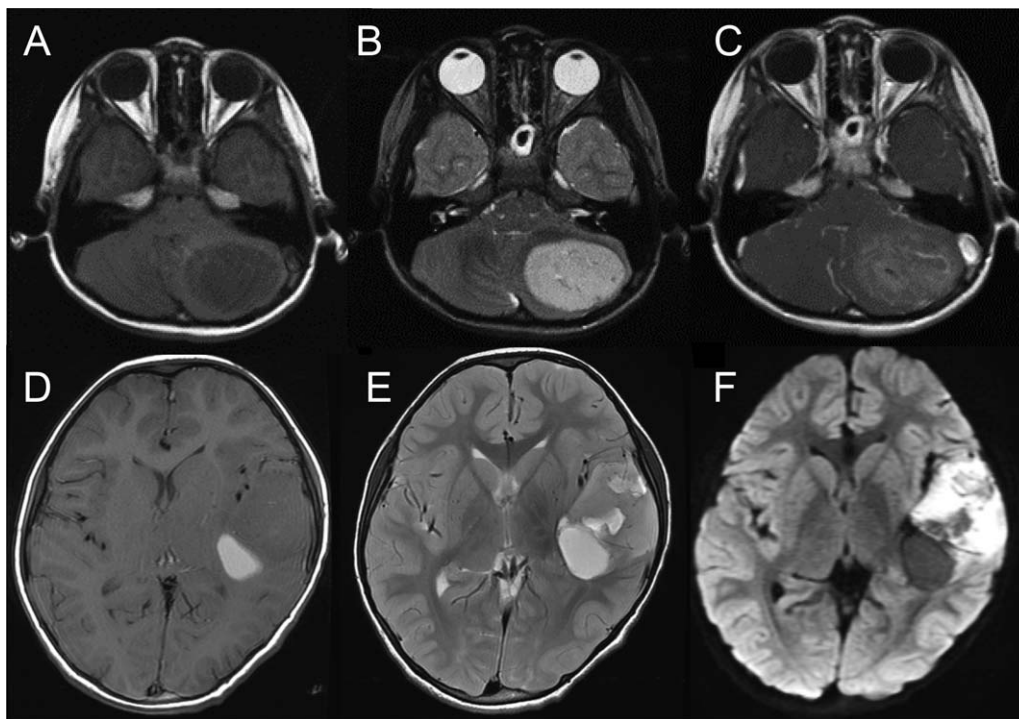
Figure 1. Radiological images of central nervous system high-grade neuroepithelial tumors with *BCOR* alteration (CNS HGNET-BCOR); **A**–**C**: case 2, **D**–**F**: case 3. The tumors presented as similar well-demarcated masses located in the cerebellar or cerebral hemispheres, hypo-intense on T1-weighted images (A, D), hyper-intense on T2-weighted images (B, E), hyper-intense on diffusion-weighted images (F) and with slight to moderate contrast enhancement (C). Partial cystic changes and intratumoral hemorrhage were also observed (D–F).

RESULTS

Clinical findings

Relevant clinical data are summarized in Table 1. The age at diagnosis ranged between 7 months and 22-year old. Of five cases with available clinical data, three cases underwent total tumor resection and intensive adjuvant chemoradiotherapies, following relatively favorable outcome over 2 years (cases 2, 3 and 5), whereas the patients in the remaining two cases died within 2 months because of the massive tumor regrowth after surgery and patient refusal of additional therapies (cases 1 and 6). In addition to local recurrence, subcutaneous seeding of the tumor was observed in case 2.

Imaging features

Magnetic resonance images of five cases (cases 1, 2, 3, 5 and 6) were studied. All five tumors exhibited similar radiographic findings. They appeared to be well-demarcated masses located in the superficial portion of the cerebral or cerebellar hemispheres. The tumors were hypo-intense on T1-weighted images (Figure 1A,D), hyper-intense on T2-weighted images (Figure 1B,E) and hyper-intense on diffusion-weighted images (Figure 1F). Varying degrees of heterogenous enhancement was observed after gadolinium injection (Figure 1C). Three of five possessed cystic components (cases 1, 3 and 5), and intratumoral hemorrhage as evidenced by T2 star sequences was observed in two cases (cases 1 and 3).

Histopathological findings

The most predominant pattern in CNS HGNET-BCOR was the compact growth of stellate tumor cells with delicate branching vessels demonstrating a chicken-wire appearance, composing most of cases 2–4 and a part of case 5 (Figure 2A,H,I). A solid growth of spindle-shaped cells in bundles with the same vascular pattern was commonly seen, being a predominant pattern in case 5 (Figure 2B). All CNS HGNET-BCOR cases exhibited, in varying degrees, microcystic formation composed of stellate cells in a myxoid and edematous background; cases 1 and 6 were mainly composed of this pattern (Figure 2C). Ependymoma-like perivascular pseudorosettes formed by the cell processes were a common finding (Figure 2D,E). Rosette-like formation containing a central area of cell processes was focally seen in cases 1, 3 and 4. A haemangiopericytoma-like stag-horn vascular pattern was focally found in case 3. Cellular fibroblastic septa commonly described in CCSK were not observed in any case (2). The interface between the tumor and normal brain parenchyma was fairly sharp in case 1 (Figure 2F), whereas microscopically minimal infiltration of isolated tumor cells was found in case 2 (Figure 2G).

Most tumor cells were stellate-shaped with scant cytoplasm, fibrillary processes and monotonous round to oval nuclei containing fine chromatin and indistinct to small nucleoli (Figure 2H). The nuclei were less chromatic than or isochromatic to those of endothelia (Figure 2H). Mild nuclear size variation was focally observed in cases 4 and 6, and slightly prominent nucleoli were found in some cells in cases 5 and 6 (Figure 2I). The cytoplasm was lightly eosinophilic to amphophilic, being less eosinophilic than that of
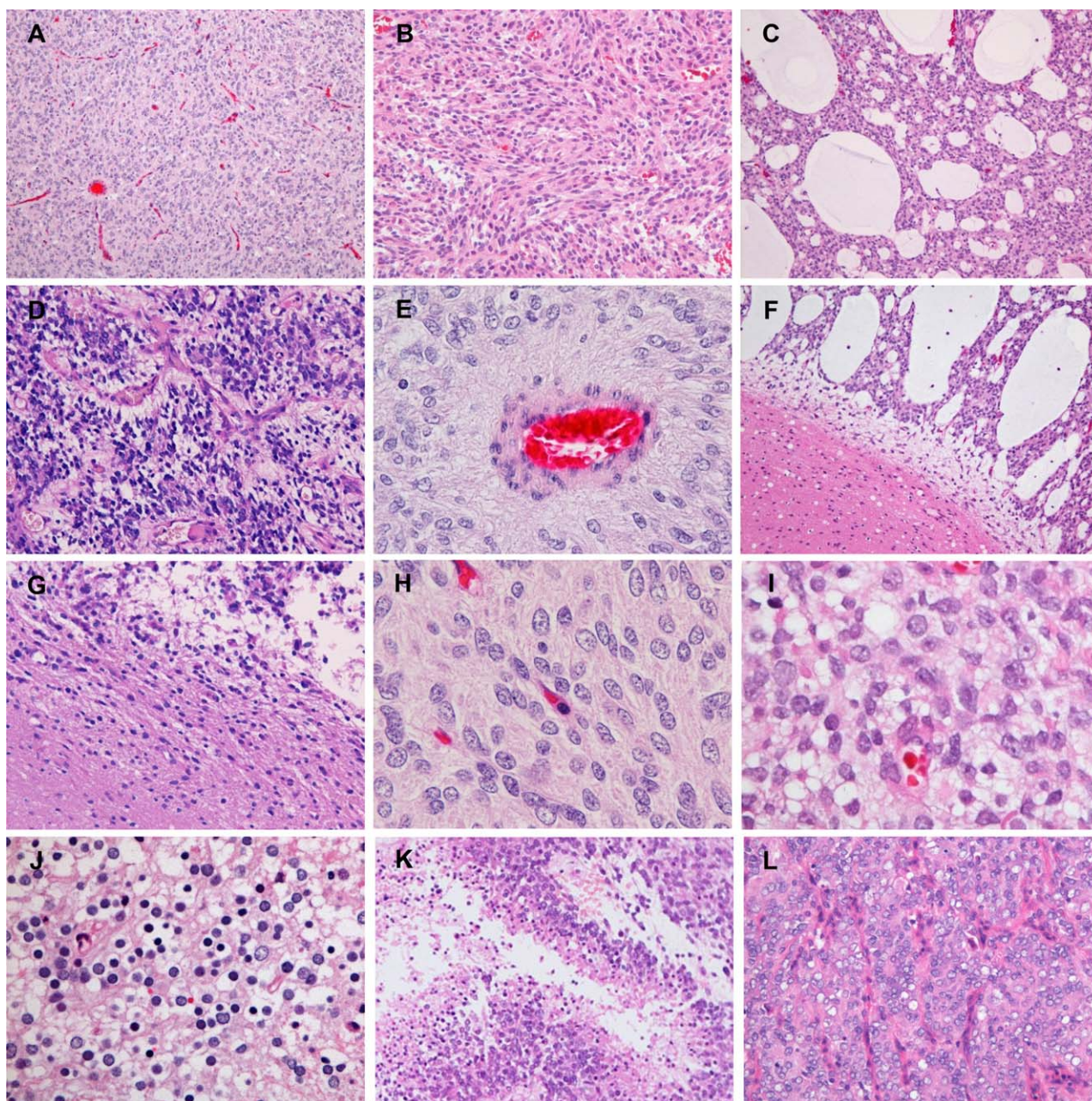
Figure 2. *Microscopic appearance of CNS HGNET-BCOR.* **A.** A compact growth of tumor cells with delicate branching vessels exhibiting a chicken-wire appearance (case 3). **B.** A solid growth of spindle-shaped cells in bundles (case 5). **C.** Microcystic formation in a myxoid and edematous background (case 1). **D, E.** Ependymoma-like perivascular pseudorosettes in cases 2 and 3, respectively. E. A perivascular anuclear zone formed by the cell processes. **F.** A sharp interface between the tumor and normal brain parenchyma (case 1). **G.** Minimal infiltration of isolated tumor cells into the surrounding brain parenchyma (case 2). **H, I.** High magnification of tumor cells. H. Tumor cells with monotonous round to oval nuclei containing fine chromatin and indistinct to small nucleoli (case 3). I. Mild nuclear size variation and some cells with slightly prominent nucleoli (case 6). **J.** Tumor cells with small, round nuclei and clear cytoplasm resembling oligodendroglioma cells and neurocytes (case 3). **K.** Palisading necrosis (case 2). **L.** A recurrent tumor from subcutaneous seeding (case 2). Original magnification: A, C, F, K, ×100; B, D, G, L, ×200; E, J, ×400; H, I, ×600.

typical neoplastic astrocytes or ependymal cells (Figure 2H,I). Tumor cells with small, round nuclei and clear cytoplasm resembling oligodendroglioma cells or neurocytes were focally found in case 3 (Figure 2J).

Mitotic counts ranged from 8 to 41 per 10 high-power fields (Table 2). Necrosis was observed in four cases, of which palisading necrosis was identified in cases 1, 2 and 4 (Figure 2K). Microvascular proliferation was not observed in any case.

Table 2. Histological and immunohistochemical features of CNS HGNET-BCOR.

Case	Perivascular pseudorosette	Necrosis	Mitosis (/10HPF)	Immunohistochemistry						EMA dot/ring-like	BCOR	MIB-1 LI (%)
				Vimentin	GFAP	Olig2	S-100 protein	Synaptophysin	NFP			
1	+	+ palisading	23	3+ (s)	1+ (s)	3+ (w-s)	1+ (s)	1+ (s)	3+ (s)	–	3+ (s)	52.7
2	+	+ palisading	24	3+ (s)	1+ (s)	2+ (w-m)	1+ (s)	–	3+ (w)	–	3+ (s)	27.8
2 (Rec)	–	+	21	NA	–	–	–	–	3+ (m)	–	3+ (s)	31.5
3	+	+ palisading	8	3+ (s)	1+ (s)	3+ (w-s)	1+ (w)	–	2+ (w)	–	3+ (m-s)	12
4	+	–	12	2+ (s)	2+ (s)	3+ (w-s)	2+ (s)	–	NA	–	3+ (w)	26.6
5	Focal	+	41	3+ (s)	2+ (s)	1+ (w-s)	1+ (s)	1+ (w)	–	–	2+ (w-m)	30.8
6	–	–	12	3+ (s)	1+ (s)	3+ (w-s)	1+ (s)	1+ (s)	1+ (s)	–	2+ (m)	43.8

The intensity and extent of immunopositive tumor cells were scored as follows: w, weak; m, moderate; s, strong; –, completely negative; 1+, <10%; 2+, 10%–50%; 3+, >50%.

Abbreviations: NA = not available; GFAP = glial fibrillary acidic protein; NFP = neurofilament protein; MIB-1 LI = MIB-1 labeling index; HPF = high power field.

The specimen from the metastasis of case 2 exhibited a solid growth of monotonous round, oval and polygonal cells with delicate branching vessels with a chicken-wire appearance separating the tumor cells into nests (Figure 2L). Stellate-shaped tumor cells with fibrillary processes and ependymoma-like perivascular pseudorosettes observed in the primary intracerebellar tumor were not evident.

The immunohistochemical findings in CNS HGNET-BCOR are summarized in Table 2. Most cases of CNS HGNET-BCOR exhibited diffuse and strong staining with vimentin (Figure 3A). GFAP immunoreactivity was identified in the cytoplasm and fibrillary processes of a small number of tumor cells (Figure 3B), but not in anuclear zones of ependymoma-like perivascular pseudorosettes. Positivity for S-100 protein was almost the same as that for GFAP (Figure 3C). All cases were immunopositive for Olig2, diffusely in most cases, with a mixture of varying degrees of intensity (Figure 3D). Immunoreactivity for synaptophysin was detected in scattered tumor cells in 3/6 cases (Figure 3E), whereas more diffuse expression of neurofilament protein was observed (Figure 3F). The reactivity for synaptophysin was not evident in the rosette-like structures. Ring-like and dot-like patterns of cytoplasmic EMA positivity were not observed in any case. Diffuse nuclear immunoreactivity for BCOR was detected in all cases (Figure 3G,H). The recurrent tumor of subcutaneous seeding in case 2 also exhibited diffuse BCOR expression. Nuclear BCOR expression was also found in the external granular layer cells in the adjacent cerebellum of case 5, but not in the internal granular layer cells (Figure 3I). Expression of INI1/BRG1 was retained in all cases. MIB-1 labeling indices ranged from 12% to 52.7%.

CCSK cases were mostly composed of round, oval and polygonal tumor cells with arborizing capillary vasculature separating the tumor cells into nests or cords (Figure 4A). Stromal sclerosis and hyalinosis, and microcystic changes were focally observed. URCS/PMMTI was composed of stellate tumor cells with microcystic formation in a myxoid background (Figure 4B). Five CCSK cases and URCS/PMMTI demonstrated diffuse BCOR expression (Figure 4C,D) and no reactivity for common glial antigens (GFAP, S-100 protein and Olig2) or synaptophysin; however, focal to diffuse expression of neurofilament protein was observed in all tumors (Figure 4E,F).

PCR and direct DNA sequencing of *BCOR* exon 15

BCOR ITD in exon 15 was confirmed in all six CNS HGNET-BCOR, five CCSK and one URCS/PMMTI by PCR and direct DNA sequencing, as shown in Figure 5. The duplicated sequences (with an insertion of 1 or 2 bp in CNS HGNET-BCOR cases 2–4 and CCSK 1) were in frame, and varied in size (90 to 114 bp), encompassing a previously reported minimally duplicated region (p.D1725 to p.L1737) (F,I).

DISCUSSION

Among *BCOR* ITD-positive tumors in the CNS, kidney and soft tissue, we here demonstrated that only CNS HGNET-BCOR exhibited neuroepithelial differentiation. Histologically, most tumor cells of CNS HGNET-BCOR exhibited glial morphology as stellate-shaped cells with fibrillary processes (Figure 2H,I). Ependymoma-
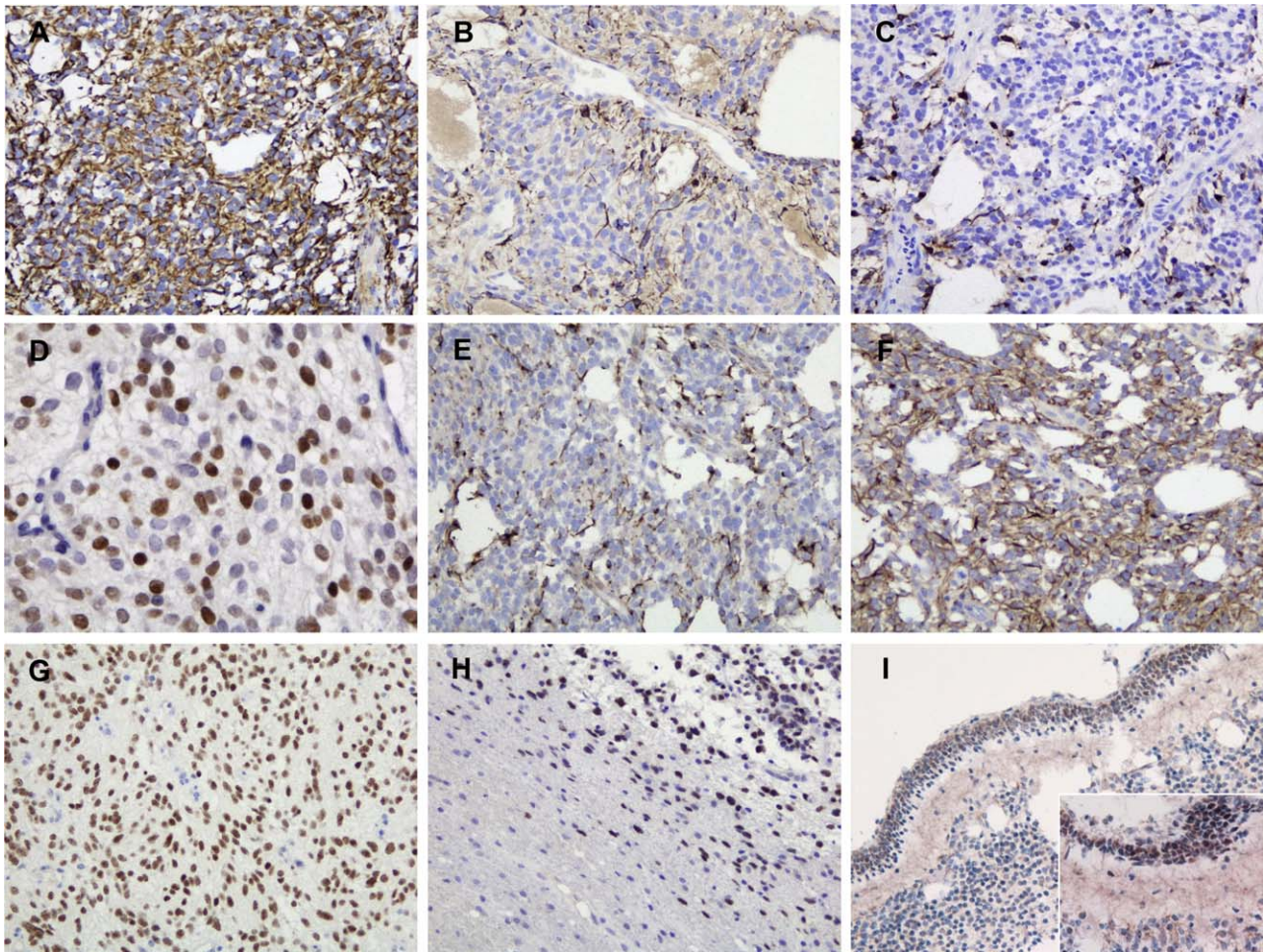
Figure 3. *Immunohistochemistry of CNS HGNET-BCOR.* **A.** Diffuse and strong positivity for vimentin (case 1). **B.** Patchy positivity for GFAP in the cytoplasm and fibrillary processes of tumor cells (case 1). **C.** Patchy positivity for S-100 protein in the cytoplasm and fibrillary processes of tumor cells (case 1). **D.** Diffuse nuclear immunoreactivity for Olig2 with a mixture of varying degrees of intensity (case 3). **E.** Scattered immunoreactivity for synaptophysin (case 1). **F.** Diffuse immunopositivity for neurofilament protein (case 1). **G.** Diffuse nuclear BCOR staining (case 3). **H.** BCOR expression highlighted isolated tumor cells infiltrating into the surrounding brain parenchyma (same area as Fig 2G; case 2). Nuclear BCOR immunopositivity was observed in the external granular layer cells in the cerebellum, but was absent in the internal granular layer cells **I.** Original magnification: A–C, E–I, ×200; D, I inset, ×400.

like perivascular pseudorosettes and palisading necrosis, the latter being characteristic of high-grade gliomas, such as glioblastomas and anaplastic ependymomas, were features of glial differentiation as well, which have not been reported in CCSK or URCS/PMMTI (Figure 2D,E,K). Although glial differentiation was not strongly supported by focal immunohistochemistry for GFAP, and S-100 protein (Table 2, Figure 3B,C), diffuse staining of Olig2 with a mixture of varying degrees of intensity was notable (Figure 3D, Table 2). Olig2 is a transcription factor required for oligodendrocyte and motor neuron development, and is commonly immunoreactive not only in glial tumors but also in glioneuronal tumors with oligodendrocyte-like cells (dysembryoplastic neuroepithelial tumors, rosette-forming glioneuronal tumors, papillary glioneuronal tumors and diffuse leptomeningeal glioneuronal tumors) (17, 21, 27) and CNS neuroblastoma with *FOXR2* activation reported by Sturm *et al* (25). Patchy Olig2 staining has been noted in CNS HGNET-BCOR in a previous study (16). URCS/PMMTI in this

study was composed of stellate tumor cells somewhat resembling neoplastic glial cells (Figure 4D); however, immunohistochemical evidence of glial differentiation was not evident. Neuronal markers, synaptophysin and neurofilament protein, were focally to diffusely positive in CNS HGNET-BCOR, whereas tumor cells with small, round nuclei and clear cytoplasm resembling neurocytes and rosette-like formations were negative for synaptophysin, suggesting that the cytomorphology and structure were not associated with neuronal differentiation. URCS/PMMTI and CCSK cases were focally to diffusely positive for neurofilament protein (Figure 4C,F), but they were negative for synaptophysin; the significance of neurofilament protein reactivity in these *BCOR* ITD-positive tumors is unknown, and the possibility of cross-reaction with other proteins cannot be ruled out.

Clinicopathologically, CNS HGNET-BCOR may be overlooked and misdiagnosed as anaplastic ependymomas, glioblastomas, medulloblastomas or CNS embryonal tumors, NOS. However,
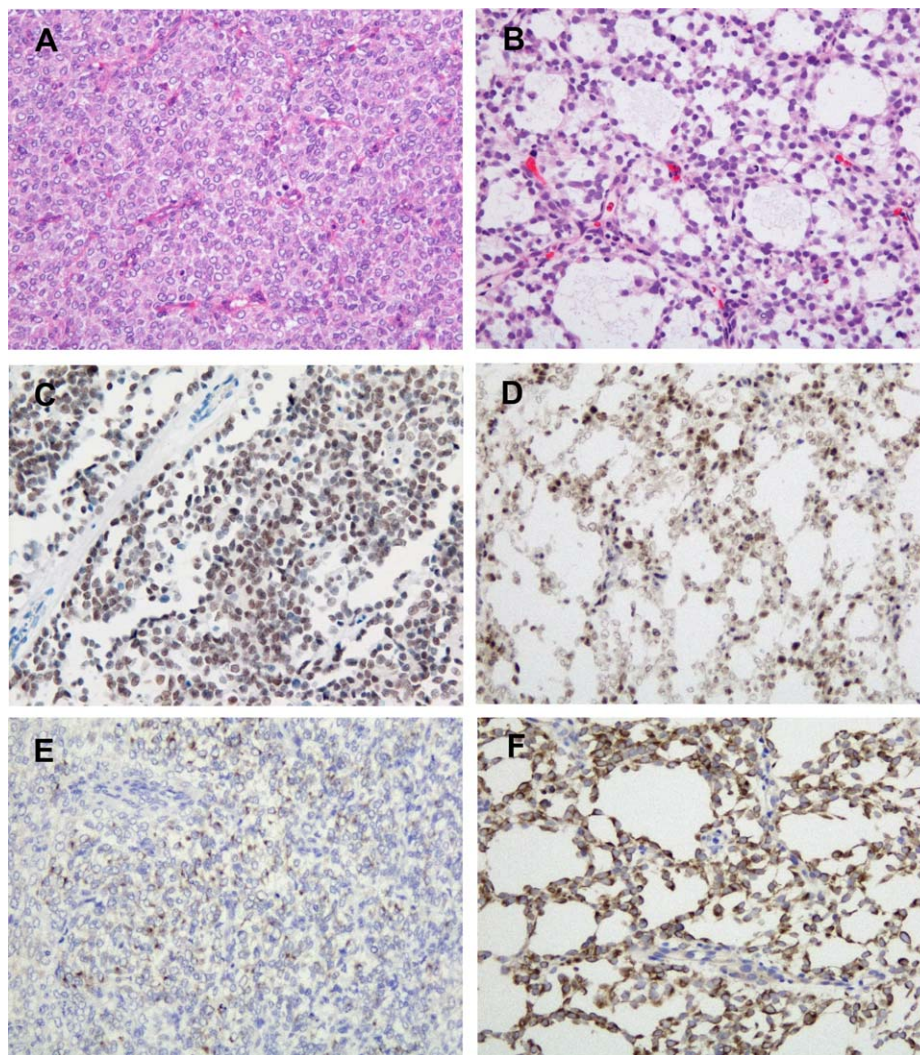
Figure 4. Histological and immunohistochemical findings of clear cell sarcomas of the kidney (CCSK) and undifferentiated round cell sarcomas/primitive myxoid mesenchymal tumors of infancy (URCS/PMMTI) (A, C, E: CCSK, B, D, F: URCS/PMMTI). **A.** The classic pattern of CCSK composed of round, oval and polygonal cells, and arborizing capillary vasculature. **B.** URCS/PMMTI case composed of stellate tumor cells with microcystic formation in a myxoid background. **C**, **D.** Diffuse nuclear immunoreactivity for BCOR. **E.** Focal immunopositivity for neurofilament protein in CCSK. **F.** Diffuse immunopositivity for neurofilament protein in URCS/PMMTI. Original magnification: A–F, ×200.

looking at the characteristic features of the nuclei is the most helpful clue in considering CNS HGNET-BCOR and ruling out these differential diagnoses exhibiting more hyperchromatic nuclei. More specifically, from our observations along with previous findings, CNS HGNET-BCOR often had ependymoma-like perivascular pseudorosettes and focal GFAP immunoreactivity; however, ring-like and dot-like patterns of cytoplasmic EMA positivity and perivascular cytoplasmic processes with GFAP immunostaining characteristic of ependymomas were not observed. Contrary with common glioblastomas, CNS HGNET-BCOR lacked nuclear pleomorphism and a diffusely infiltrative growth pattern, and cytological and immunohistochemical evidence of glial differentiation were weaker. CNS HGNET-BCOR often occurred in the cerebellum (16/25, 56%) (Supporting Information Table S1); therefore, medulloblastomas, as well as ependymomas, were considered. Unlike CNS embryonal tumors, such as medulloblastomas, the typical embryonal morphology—a highly cellular, poorly differentiated, hyperchromatic and mitotically active histological appearance reminiscent of the developing embryonic nervous system—was not observed, and neuronal differentiation was not evident in CNS HGNET-BCOR.

Santiago et al noted similarities between BCOR ITD-positive tumors and malignant rhabdoid tumors (MRT) with INI1/BRG1 deficiency: similar morphological features among each tumor group, tumor locations in the CNS, soft tissue and kidney, and age distribution with most occurring in infants (24). However, unlike extra-CNS MRT, CNS MRT, that is, atypical teratoid/rhabdoid tumors (AT/RT), are usually not composed solely or even largely of rhabdoid cells, and their typical histology is a jumbled appearance created by epithelioid tumor cells with variability of
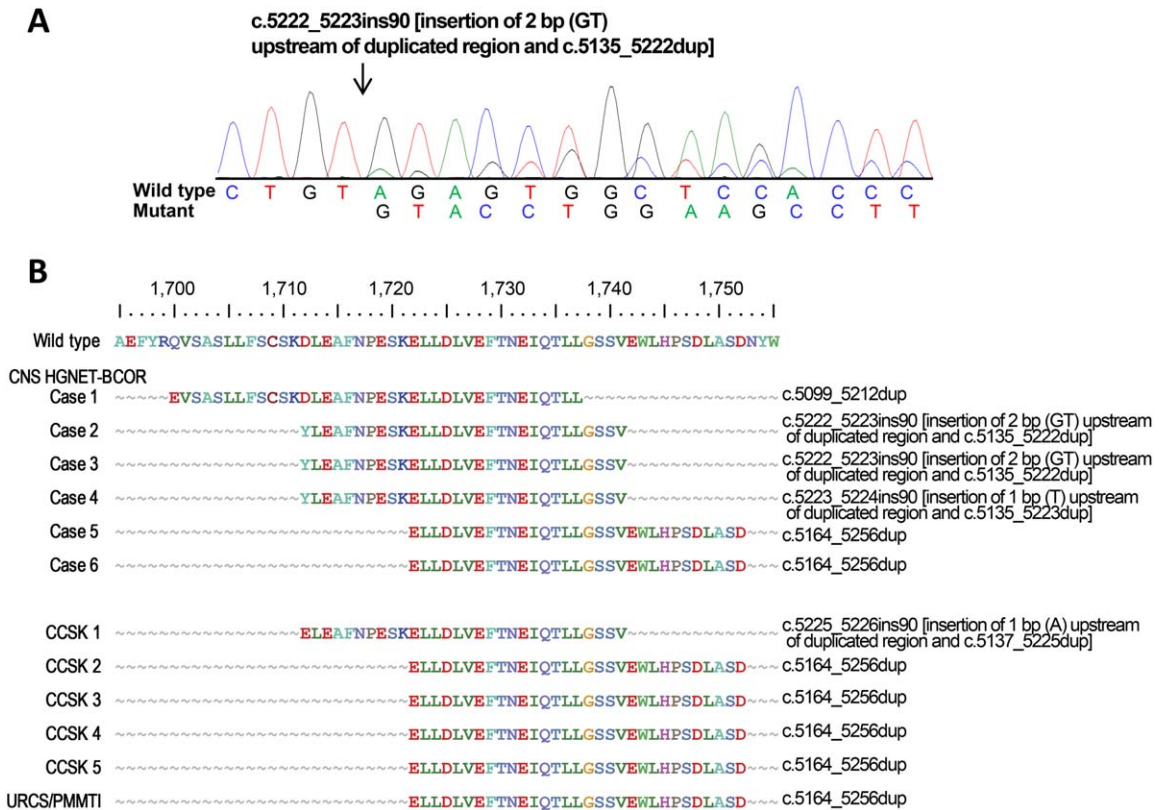
Figure 5. BCOR *exon 15 aberrations in* BCOR *ITD-positive tumors.* **A.** An example of the duplicated coding sequence of CNS HGNET-BCOR in case 3. The 2-bp insertion and 88-bp tandem duplication are illustrated. The nucleotide position is relative to the sequence used as the reference (NM_001123385.1). **B.** Predicted protein sequences of duplicated regions and genetic changes in the CNS HGNET, CCSK and URCS/PMMTI. At the top, the wild-type BCOR amino acid sequence from positions 1695 to 1755 is presented (NP_001116857).

cytoplasmic features—scant, eosinophilic, pale, clear or vacuolated—with the presence of rhabdoid cells (5, 22). Therefore, *BCOR* ITD-positive tumors and MRT are more similar in that, among each tumor group, CNS tumors exhibit unique histological features. From a genetic standpoint, soft tissue MRT have a higher incidence of homozygous deletion of the *INI* gene than AT/RT and renal MRT, and the mutation hotspots in the gene are exons 5 and 9 in AT/RT, whereas mutations in exon 2 are common in renal MRT (4, 9). As for *BCOR* ITD-positive tumors, although the minimally duplicated region (p.D1725 to p.L1737) were common, the altered amino acid sequence pattern found in cases 2–4, combined with previous studies, has been observed in 4 of 25 (16%) CNS HGNET-BCOR, which has not been seen so far in CCSK or URCS/PMMTI, and duplicated regions extending toward the N-end from p.Asp1712 were more common in CNS HGNET-BCOR (Figure 5, Supporting Information Fig. S1). However, the numbers of reported CNS HGNET-BCOR and URCS/PMMTI are lower than that of CCSK (176 cases) (3, 12, 14, 15, 23, 26).

Case 2 exhibited subcutaneous seeding 16 months after the first operation (Table 1). In the resected metastasis, tumor cells lost fibrillary cytoplasmic processes, and ependymoma-like perivascular pseudorosettes and expression of glial markers observed in the primary tumor were not evident (Figure 2D,L, Table 2). Moreover, in a case of CNS HGNET-BCOR reported by Paret *et al*, three inoculation metastases developed at the skullcap, and the metastatic tumor lost the perivascular pseudorosettes observed in the primary tumor. Chemotherapy and radiotherapy performed after the first surgery may be responsible for these morphological and phenotypical changes; however, the possibility of effects of intracranial environment on neuroepithelial differentiation of the tumors cannot be ruled out.

BCOR immunohistochemical expression has been tested in normal tissues including the spleen, placenta, kidney, colon, liver, skin, pancreas, testis, lung and brain (1, 13), and only spermatogonia in the seminiferous tubules of the normal testis were found to exhibit distinct nuclear staining (13). In this study, using the same anti-BCOR monoclonal antibody, we found nuclear BCOR expression in the external granular layer cells in the adjacent cerebellum of case 5, but not in the internal granular layer cells, which was confirmed by staining of other unrelated surgical specimens containing the normal cerebellar external granular layer (Figure 3I). The specificity of immunohistochemical nuclear expression of BCOR in other CNS tumors, especially desmoplastic/nodular medulloblastomas and medulloblastomas with extensive nodularity, whose development is thought to be associated with the cerebellar external granular layer (7), needs to be investigated.

A nosological issue is how CNS HGNET-BCOR should be classified in the current World Health Organization (WHO) scheme of CNS tumors. Although the age distribution is similar with that of the category of "embryonal tumors," the typical embryonal

morphology and evident neuronal differentiation were not observed; therefore, we believe that CNS HGNET-BCOR do not belong in "embryonal tumors." Although their counterparts in the kidney and soft tissue are classified as "sarcomas," CNS HGNET-BCOR exhibited cytological and immunohistochemical evidence of neuroepithelial differentiation, thus CNS HGNET-BCOR do not fit in the category of "mesenchymal, non-meningothelial tumors," either. A new category, in which CNS HGNET-BCOR will be classified, may be established in the next WHO scheme of CNS tumors. However, given the small number of cases examined in the current study, further clinicopathological and genetic analyses on more cases are needed.

ACKNOWLEDGMENT

CONFLICT OF INTEREST

The authors have no conflict of interest.

REFERENCES

1. Appay R, Macagno N, Padovani L, Korshunov A, Kool M, André N *et al* (2017) HGNET-BCOR tumors of the cerebellum: clinicopathologic and molecular characterization of 3 cases. *Am J Surg Pathol* **41**:1254–1260.

2. Argani P, Perlman EJ, Breslow NE, Browning NG, Green DM, D'Angio GJ *et al* (2000) Clear cell sarcoma of the kidney: a review of 351 cases from the National Wilms Tumor Study Group Pathology Center. *Am J Surg Pathol* **24**:4–18.

3. Astolfi A, Melchionda F, Perotti D, Fois M, Indio V, Urbini M *et al* (2015) Whole transcriptome sequencing identifies BCOR internal tandem duplication as a common feature of clear cell sarcoma of the kidney. *Oncotarget* **6**:40934–40939.

4. Biegel JA (2006) Molecular genetics of atypical teratoid/rhabdoid tumor. *Neurosurg Focus* **20**:E11.

5. Burger PC, Yu IT, Tihan T, Friedman HS, Strother DR, Kepner JL *et al* (1998) Atypical teratoid/rhabdoid tumor of the central nervous system: a highly malignant tumor of infancy and childhood frequently mistaken for medulloblastoma: a Pediatric Oncology Group study. *Am J Surg Pathol* **22**:1083–1092.

6. Chiang S, Lee CH, Stewart CJR, Oliva E, Hoang LN, Ali RH *et al* (2017) BCOR is a robust diagnostic immunohistochemical marker of genetically diverse high-grade endometrial stromal sarcoma, including tumors exhibiting variant morphology. *Mod Pathol* **30**:1251–1261.

7. Ellison DW, Eberhart CG, Pietsch T, Pfister S (2016) Medulloblastoma. In: *WHO Classification of Tumors of the Central Nervous System, Revised*, 4th edn. DN Louis, H Ohgaki, OD Wiestler, WK Cavenee (eds), pp. 184–200. IARC Press: Lyon, France.

8. Furtwängler R, Gooskens SL, van Tinteren H, de Kraker J, Schleiermacher G, Bergeron C *et al* (2013) Clear cell sarcomas of the kidney registered on International Society of Pediatric Oncology (SIOP) 93–01 and SIOP 2001 protocols: a report of the SIOP Renal Tumour Study Group. *Eur J Cancer* **49**:3497–3506.

9. Geller JI, Roth JJ, Biegel JA (2015) Biology and treatment of rhabdoid tumor. *Crit Rev Oncog* **20**:199–216.

10. Gooskens SL, Furtwängler R, Spreafico F, van Tinteren H, de Kraker J, Vujanic GM *et al* (2014) Treatment and outcome of patients with relapsed clear cell sarcoma of the kidney: a combined SIOP and AIEOP study. *Br J Cancer* **111**:227–233.

11. Ikota H, Nobusawa S, Arai H, Kato Y, Ishizawa K, Hirose T *et al* (2015) Evaluation of IDH1 status in diffusely infiltrating gliomas by immunohistochemistry using anti-mutant and wild type IDH1 antibodies. *Brain Tumor Pathol* **32**:237–244.

12. Kao YC, Sung YS, Zhang L, Huang SC, Argani P, Chung CT *et al* (2016) Recurrent BCOR Internal tandem duplication and YWHAE-NUTM2B fusions in soft tissue undifferentiated round cell sarcoma of infancy: overlapping genetic features with clear cell sarcoma of kidney. *Am J Surg Pathol* **40**:1009–1020.

13. Kao YC, Sung YS, Zhang L, Jungbluth AA, Huang SC, Argani P *et al* (2016) BCOR overexpression is a highly sensitive marker in round cell sarcomas with BCOR genetic abnormalities. *Am J Surg Pathol* **40**: 1670–1678.

14. Karlsson J, Valind A, Gisselsson D (2016) BCOR internal tandem duplication and YWHAE-NUTM2B/E fusion are mutually exclusive events in clear cell sarcoma of the kidney. *Genes Chromosomes Cancer* **55**:120–123.

15. Kenny C, Bausenwein S, Lazaro A, Furtwängler R, Gooskens SL, van den Heuvel Eibrink M *et al* (2016) Mutually exclusive BCOR internal tandem duplications and YWHAE-NUTM2 fusions in clear cell sarcoma of kidney: not the full story. *J Pathol* **238**:617–620.

16. Kline CN, Joseph NM, Grenert JP, van Ziffle J, Talevich E, Onodera C *et al* (2017) Targeted next-generation sequencing of pediatric neuro-oncology patients improves diagnosis, identifies pathogenic germline mutations, and directs targeted therapy. *Neuro Oncol* **19**:699–709.

17. Matsumura N, Yokoo H, Mao Y, Yin W, Nakazato Y (2013) Olig2-positive cells in glioneuronal tumors show both glial and neuronal characters: the implication of a common progenitor cell?. *Neuropathology* **33**:246–255.

18. Nakazato Y, Ishizeki J, Takahashi K, Yamaguchi H, Kamei T, Mori T (1982) Localization of S-100 protein and glial fibrillary acidic protein-related antigen in pleomorphic adenoma of the salivary glands. *Lab Invest* **46**:621–626.

19. O'Meara E, Stack D, Lee CH, Garvin AJ, Morris T, Argani P *et al* (2012) Characterization of the chromosomal translocation t(10;17)(q22;p13) in clear cell sarcoma of kidney. *J Pathol* **227**: 72–80.

20. Paret C, Theruvath J, Russo A, Kron B, El Malki K, Lehmann N *et al* (2016) Activation of the basal cell carcinoma pathway in a patient with CNS HGNET-BCOR diagnosis: consequences for personalized targeted therapy. *Oncotarget* **7**:83378–83391.

21. Rodriguez FJ, Perry A, Rosenblum MK, Krawitz S, Cohen KJ, Lin D *et al* (2012) Disseminated oligodendroglial-like leptomeningeal tumor of childhood: a distinctive clinicopathologic entity. *Acta Neuropathol* **124**:627–641.

22. Rorke LB, Packer RJ, Biegel JA (1996) Central nervous system atypical teratoid/rhabdoid tumors of infancy and childhood: definition of an entity. *J Neurosurg* **85**:56–65.

23. Roy A, Kumar V, Zorman B, Fang E, Haines KM, Doddapaneni H *et al* (2015) Recurrent internal tandem duplications of BCOR in clear cell sarcoma of the kidney. *Nat Commun* **6**:8891.

24. Santiago T, Clay MR, Allen SJ, Orr BA (2017) Recurrent BCOR internal tandem duplication and BCOR or BCL6 expression distinguish primitive myxoid mesenchymal tumor of infancy from congenital infantile fibrosarcoma. *Mod Pathol* **30**:884–891.

25. Sturm D, Orr BA, Toprak UH, Hovestadt V, Jones DTW, Capper D *et al* (2016) New brain tumor entities emerge from molecular classification of CNS-PNETs. *Cell* **164**:1060–1072.

26. Ueno-Yokohata H, Okita H, Nakasato K, Akimoto S, Hata J, Koshinaga T *et al* (2015) Consistent in-frame internal tandem duplications of BCOR characterize clear cell sarcoma of the kidney. *Nat Genet* **47**:861–863.

27. Yokoo H, Nobusawa S, Takebayashi H, Ikenaka K, Isoda K, Kamiya M *et al* (2004) Anti-human Olig2 antibody as a useful immunohistochemical marker of normal oligodendrocytes and gliomas. *Am J Pathol* **164**:1717–1725.

SUPPORTING INFORMATION

Additional Supporting Information may be found in the online version of this article at the publisher's web-site:

Figure S1. Diagram of inferred BCOR protein sequences from *BCOR* ITD-positive tumors. The dataset was composed of 204 *BCOR* ITD-positive tumors from 11 publications and our cohort (6 CNS HGNET, 5 CCSK and 1 URCS/PMMTI). The frequent duplication patterns in each tumor type are expressed as percentages. Arrowhead indicates p.Asp1712.
*Duplication patterns found only in CNS HGNET-BCOR

Table S1. Comparative clinical features of BCOR ITD-positive tumors.